

Magnetic properties of the three-dimensional Hubbard model at half filling.

Anne-Marie Daré¹, and Gilbert Albinet

I.R.P.H.E., UMR 6594

Université de Provence, Campus de St Jérôme, Case 252

13397 Marseille Cedex 20, France

(14 septembre 1999)

We study the magnetic properties of the 3d Hubbard model at half-filling in the TPSC formalism, previously developed for the 2d model. We focus on the Néel transition approached from the disordered side and on the paramagnetic phase. We find a very good quantitative agreement with Dynamical Mean-Field results for the isotropic 3d model. Calculations on finite size lattices also provide satisfactory comparisons with Monte Carlo results up to the intermediate coupling regime. We point out a qualitative difference between the isotropic 3d case, and the 2d or anisotropic 3d cases for the double occupation factor. Even for this local correlation function, 2d or anisotropic 3d cases are out of reach of DMF: this comes from the inability of DMF to account for antiferromagnetic fluctuations, which are crucial.

I. INTRODUCTION

The problem of strongly correlated fermions is a long-standing open question. Recently progress in the resolution of the simplest model, namely the Hubbard model in $d = \infty$ by the Dynamical Mean Field approach (DMF), [1] [2] marked a real breakthrough in the field. Nevertheless, the lack of spatial dependence and the difficulties in including the $1/d$ corrections, [2] and the low dimensionality or the anisotropic character of the experimental systems, justify the ongoing research on more realistic dimensions $d = 2$ and 3 . In low dimension, especially $d = 2$, one expects a strong \mathbf{k} -dependence of the self-energy that is absent from $d = \infty$ calculations. In this paper we study the 3d isotropic Hubbard model, using a formalism previously developed in 2d, [3] [4] named TPSC for Two Particle Self Consistent. In 2d, the TPSC approach has been shown to give reliable results in comparisons with Monte Carlo calculations for one and two-particle properties, static and dynamical quantities, for a whole range of parameters: for a general band filling, on the whole temperature range accessible to Monte Carlo simulations (but probably not at very low temperature at half-filling in $2d$), from low up to intermediate value of U/W , for the nearest neighbor model as well as for the Utt' case. [5] The strengths of this approach rely on the respect of several benchmark properties: it fulfills the Pauli principle and is conserving in the Baym and Kadanoff sense. [6] It was shown in 2d to satisfy the Mermin-Wagner theorem. Furthermore the TPSC approach is appealing due to its simplicity: the vertices retained in the particle-hole channels are static and local.

Apart from the 2d case, the highly anisotropic 3d case (inter-plane hopping much less than in-plane one) has been studied previously. [7] It was found that the antiferromagnetic order can be established in the regime of incoherent 3d one-particle motion and the crossover between 2 and 3d was studied in details. In this paper we want to explore the magnetic properties of the isotropic 3d model, focusing on the paramagnetic phase and on the Néel transition approached from the disordered side. We make comparisons with other approaches, including Monte Carlo results, and DMF approach for the hypercubic lattice. We also stress the qualitative difference between isotropic and anisotropic 3d cases, even for a local function as the double occupation factor.

The paper is organized as follows: In Sec. II we review the TPSC formalism for the particle-hole properties, namely spin and charge susceptibilities. Sec. III concerns the Néel transition, and Sec. IV is devoted to the temperature dependence of the double occupation factor from which all the magnetic properties follow. Finally we summarize our conclusions in Sec. V. An appendix details the calculation of the double occupation factor for a simple two-site model that enlightens the high-temperature lattice results.

II. TWO-PARTICLE SELF-CONSISTENT FORMALISM

We start from the Hubbard Hamiltonian,

$$H = - \sum_{\langle ij \rangle \sigma} t_{i,j} \left(c_{i\sigma}^\dagger c_{j\sigma} + c_{j\sigma}^\dagger c_{i\sigma} \right) + U \sum_i n_{i\uparrow} n_{i\downarrow} - \mu \sum_{i\sigma} n_{i\sigma} , \quad (1)$$

where the operator $c_{i\sigma}$ ($c_{i\sigma}^\dagger$) destroys (creates) an electron of spin σ at site i , $n_{i\sigma}$ is the density operator, and $t_{i,j}$ is the symmetric hopping matrix. The on-site repulsion U is the screened Coulomb interaction, μ the chemical potential. For a while hopping parameters will be kept general. Indeed the Two-Particle Self-Consistent formalism (TPSC) approach only requires a local interaction but can be applied to a general band structure.

Let us sketch the TPSC approach, fully developed in Ref. [3] and [4]. The TPSC can be formulated in a closed form in the functional integral formalism. [4] Here we shall concentrate on the two-particle properties, and obtain the useful relations in the equation of motion approach. In the presence of a time, space and spin varying external field ϕ , a generalized Green function can be defined: [8]

$$G(r_i, r_j, \tau_i; \phi) = \frac{\text{Tr} \left[e^{-\beta H} T_\tau S(\beta) c_{i\sigma}^\dagger(\tau_i) c_{j\sigma}(\tau_i) \right]}{\text{Tr} \left[e^{-\beta H} T_\tau S(\beta) \right]}, \quad (2)$$

where T_τ means imaginary time ordering and

$$\ln S(\beta) = - \int_0^\beta d\tau \sum_{l,\sigma} c_{l\sigma}^\dagger(\tau) c_{l\sigma}(\tau) \phi_\sigma(l, \tau) . \quad (3)$$

All the field dependence is in $S(\beta)$ and

$$c_{l\sigma}^\dagger(\tau) = e^{\tau H} c_{l\sigma}^\dagger e^{-\tau H} . \quad (4)$$

To obtain the spin and charge susceptibilities, the equation of motion for G has to be evaluated. Then in the linear response theory, the functional derivative with respect to ϕ is taken at zero field leading to:

$$\delta \left(\frac{\partial \langle c_{i\sigma}^\dagger c_{j\sigma} \rangle}{\partial \tau_i} \right) = (\delta \phi_\sigma(i, \tau_i) - \delta \phi_\sigma(j, \tau_i)) \langle c_{i\sigma}^\dagger c_{j\sigma} \rangle \Big|_{\phi=0} + U \delta \langle c_{i\sigma}^\dagger c_{j\sigma} n_{l\bar{\sigma}} (\delta_{i,l} - \delta_{j,l}) \rangle + \delta C , \quad (5)$$

with the kinetic part

$$\delta C = \frac{1}{N} \sum_{\mathbf{k}\mathbf{q}} (\epsilon_{\mathbf{k}} - \epsilon_{\mathbf{k}+\mathbf{q}}) e^{-i\mathbf{k}\mathbf{r}_i} e^{i(\mathbf{k}+\mathbf{q})\mathbf{r}_j} \delta \langle c_{\mathbf{k}\sigma}^\dagger c_{\mathbf{k}+\mathbf{q}\sigma} \rangle . \quad (6)$$

All the operators in Eqs. (5) and (6) are at the same time τ_i and $\langle \dots \rangle$ is a short-hand notation for averaging with $S(\beta)$ as in Eq. (2). $\bar{\sigma}$ is opposite to σ , \mathbf{k} is a wave vector of an N -site lattice, and $\epsilon_{\mathbf{k}}$ is the Fourier transform of $t_{i,j}$.

The ansatz of the TPSC approach is to write, for the term proportional to U in Eq.(5), that the following approximation retains the main correlation effects:

$$\delta \langle c_{i\sigma}^\dagger c_{j\sigma} n_{l\bar{\sigma}} \rangle \simeq \delta \left(g_{\sigma\bar{\sigma}}(l, \tau_i) \langle c_{i\sigma}^\dagger c_{j\sigma} \rangle \langle n_{l\bar{\sigma}} \rangle \right) \quad \text{for } l = i \text{ or } l = j , \quad (7)$$

with the following definition:

$$g_{\sigma\bar{\sigma}}(l, \tau_i) = \frac{\langle n_{l\sigma}(\tau_i) n_{l\bar{\sigma}}(\tau_i) \rangle}{\langle n_{l\sigma}(\tau_i) \rangle \langle n_{l\bar{\sigma}}(\tau_i) \rangle} \quad (8)$$

Eq. (7) is exact when $i = j$. The expansion of the functional derivative with respect to ϕ leads to

$$U \delta \langle c_{i\sigma}^\dagger c_{j\sigma} (n_{i\bar{\sigma}} - n_{j\bar{\sigma}}) \rangle = U \langle c_{i\sigma}^\dagger c_{j\sigma} \rangle \Big|_{\phi=0} \left\{ \langle n_{i\bar{\sigma}} \rangle \Big|_{\phi=0} (\delta g_{\sigma\bar{\sigma}}(i, \tau_i) - \delta g_{\sigma\bar{\sigma}}(j, \tau_i)) + g_{\sigma\bar{\sigma}} \Big|_{\phi=0} (\delta \langle n_{i\bar{\sigma}} \rangle - \delta \langle n_{j\bar{\sigma}} \rangle) \right\} , \quad (9)$$

since at zero field in the paramagnetic phase, the coefficient of the term proportional to $\delta \langle c_{i\sigma}^\dagger c_{j\sigma} \rangle$ cancels.

To get the spin susceptibility it remains to take $\phi_\sigma(i, \tau_i) = \sigma \phi(i, \tau_i)$, then to time- and site-Fourier transform Eq.(5), using Eqs.(6) to (9). From the definition

$$\chi_{sp}(q, i\omega_q) = - \frac{1}{N} \sum_{\mathbf{k}} \frac{\delta \langle \sum_{\sigma} \sigma c_{\mathbf{k}\sigma}^\dagger c_{\mathbf{k}+\mathbf{q}\sigma} \rangle_{i\omega_q}}{\delta \phi(q, i\omega_q)} \quad (10)$$

the preceding equations lead to an effective RPA expression for the spin susceptibility

$$\chi_{sp}(q, i\omega_q) = \frac{\chi_0(q, i\omega_q)}{1 - \frac{1}{2}U_{sp}\chi_0(q, i\omega_q)} , \quad (11)$$

with

$$U_{sp} = g_{\uparrow\downarrow}U . \quad (12)$$

$g_{\uparrow\downarrow}$ is the time- and site-independent version of Eq.(8). This q and $i\omega_q$ independence follows from the cancellation of the term proportional to $\delta g_{\sigma\bar{\sigma}}$ which does not depend on the spin index, and disappears by summation on σ : $\sum_{\sigma} \sigma \delta g_{\sigma\bar{\sigma}} = 0$. As will be recalled later, $g_{\uparrow\downarrow}$ can be evaluated in a self-consistent equation dictated by sum rules. For the charge susceptibilities the term proportional to $\delta g_{\sigma\bar{\sigma}}$ doesn't cancel, and one obtains a \mathbf{q} and $i\omega_q$ -dependent renormalized interaction. However further simplification consisting in taking a \mathbf{q} and $i\omega_q$ -constant renormalized vertex for charge $U_{ch} = (g_{\uparrow\downarrow} + \delta g)U$, where δg can be self-consistently evaluated using exact sum rules, has been shown to give reasonable results in comparison to Monte Carlo simulations. The sum rules to determine self-consistently U_{sp} and U_{ch} follow from the the Pauli principle and the fluctuation-dissipation theorem, here expressed in Matsubara formalism

$$\langle S_i^z S_i^z \rangle = \langle (n_{\uparrow} - n_{\downarrow})^2 \rangle = n - 2 \langle n_{\uparrow} n_{\downarrow} \rangle = \frac{1}{\beta N} \sum_{\mathbf{q}, i\omega_q} \frac{\chi_0(\mathbf{q}, i\omega_q)}{1 - \frac{1}{2}U_{sp}\chi_0(\mathbf{q}, i\omega_q)} , \quad (13)$$

and

$$\langle \delta n_i \delta n_i \rangle = n + 2 \langle n_{\uparrow} n_{\downarrow} \rangle - n^2 = \frac{1}{\beta N} \sum_{\mathbf{q}, i\omega_q} \frac{\chi_0(\mathbf{q}, i\omega_q)}{1 + \frac{1}{2}U_{ch}\chi_0(\mathbf{q}, i\omega_q)} , \quad (14)$$

where $\beta \equiv 1/T$, $n = \langle n_{\uparrow} \rangle + \langle n_{\downarrow} \rangle$, and $\delta n_i = \sum_{\sigma} n_{i\sigma} - n$. The necessity to have two different irreducible vertices for spin and charge is imposed by the Pauli principle. Simple RPA for which the spin and charge susceptibilities differ only by a sign in the denominator cannot fulfill these previous rules.

Although the susceptibilities have an RPA functional form, the physical properties of the theory are very different from RPA because of the self-consistency conditions for determining U_{sp} and U_{ch} . This approach has been shown [3] to take into account both the local quantum renormalization effects (Kanamori-Brueckner screening) which reduce the Coulomb repulsion, and long-wavelength thermal fluctuations, giving a phase transition only at zero-temperature in two dimensions. This theory is self-consistent at the two-particle level (hence its name), in contrast with FLEX [9] for example, which is self-consistent at the one-particle level.

In this paper we shall concentrate on magnetic properties for the nearest-neighbor model on a 3d-simple cubic lattice with a spacing $a = 1$, for which the dispersion relation reads

$$\epsilon_{\mathbf{k}} = -2t \sum_{i=1}^3 \cos k_i , \quad (15)$$

with a bandwidth $W = 12t$. The numerics only concern the half-filled band case, hence $\chi_0(\mathbf{q}, 0)$ is maximum at $\mathbf{Q} = (\pi, \pi, \pi)$ due to the perfect nesting. The calculations are done on a variable mesh for the Brillouin zone: 16^3 on the coarse one, 16^3 more points near \mathbf{Q} , but as will be detailed below, some integrals are analytically evaluated, and the non-interacting susceptibility is finely evaluated at low temperature. We also present calculations on finite-size lattice for comparisons with Monte Carlo results. Hereafter t will be the energy unit, and we set $k_B = 1$.

III. THE ANTIFERROMAGNETIC TRANSITION

The TPSC formalism has been shown to give reliable results far from the transition and also in the part of the critical regime that is accessible to Monte Carlo calculations. Important constraints such as the Mermin-Wagner theorem are fulfilled by the TPSC approach. Indeed in 2d as the temperature goes down, U_{sp} decreases, thus preventing a finite-temperature magnetic transition. However deep in the low temperature regime at half-filling in 2d, the relation $U_{sp} = U g_{\uparrow\downarrow}$ breaks down: there is no reason to believe that there is no double-occupied site in the ground state. [4] In the highly anisotropic three-dimensional case with a small inter-plane hopping $t_z \ll t$, a finite-temperature transition

can be stabilized. Here we shall concentrate on the isotropic case and make comparisons with other approaches developed for the 3d or for the infinite-dimensional Hubbard model.

In 3d, at half filling, the self-consistent Eq.(13) from which the magnetic properties will be evaluated, can be rewritten

$$1 - \frac{1}{2}g_{\uparrow\downarrow} = T \int \frac{d^3q}{(2\pi)^3} \chi_{sp}^{as}(\mathbf{q}, 0) + T \int \frac{d^3q}{(2\pi)^3} (\chi_{sp}(\mathbf{q}, 0) - \chi_{sp}^{as}(\mathbf{q}, 0)) + T \int \frac{d^3q}{(2\pi)^3} \sum_{i\omega_q \neq 0} \chi_{sp}(\mathbf{q}, i\omega_q), \quad (16)$$

where $\chi_{sp}^{as}(\mathbf{q}, 0)$ is the asymptotic form of $\chi_{sp}(\mathbf{q}, 0)$ obtained from a Taylor expansion around \mathbf{Q} of the denominator and defined on a domain of radius Λ around \mathbf{Q} . This enables an analytic evaluation of the diverging part of the susceptibility. Defining $U_{mfc} = 2/\chi_0(\mathbf{Q}, 0)$ the mean-field critical value of U at which the transition occurs in a RPA treatment, and $\delta U = U_{mfc} - U_{sp}$ the small energy scale that measures the proximity to the phase transition in the TPSC approach, the asymptotic form of the spin susceptibility simply reads

$$\chi_{sp}^{as}(\mathbf{q}, 0) = \frac{2}{\delta U} \frac{1}{1 + \xi^2 \left[(q_x - \pi)^2 + (q_y - \pi)^2 + (q_z - \pi)^2 \right]}, \quad (17)$$

where ξ is the magnetic correlation length defined in terms of a microscopic length ξ_0 :

$$\xi^2 = \xi_0^2 \frac{U_{sp}}{\delta U} \quad (18)$$

$$\xi_0^2 = \frac{1}{4} U_{mfc} \left| \frac{\partial^2 \chi_0}{\partial q_x^2} \right|_{\mathbf{q}=\mathbf{Q}}. \quad (19)$$

The Néel transition is reached from above when $U_{sp} \rightarrow U_{mfc}^-$. The TPSC approach validity is restricted from low up to intermediate value of the ratio U/W . Indeed it has been shown, and will be confirmed below, that U_{sp} saturates at strong coupling while one would expect U_{sp} to have a maximum as a function of U , as suggested by RPA at low repulsion and by the Heisenberg model limit at strong repulsion. Nevertheless the reliability for $U \lesssim W$ in 2d has been established by comparisons with Monte Carlo calculations, and gives some confidence in 3d for the intermediate coupling regime.

Fig.1 presents T_N as a function of U in units of the hopping parameter $t = 1$. TPSC results are presented along with Monte Carlo, [10] RPA, dynamical mean field results on an hypercubic lattice, [11] [12] spin-fluctuation formalism, [13] and spin Hamiltonian approach. [14] [15] The last one is a mapping of the Hubbard model onto an Heisenberg model with arbitrary-range, U-dependent exchange integrals $J_{ij}(U)$, treated in an Onsager reaction field method. The DMF results are scaled for comparisons with 3d by $\sqrt{\langle \epsilon_k^2 \rangle}$ (details will be given in next section).

Usual RPA predicts an exponential behavior:

$$T_N^{RPA} = \Gamma \exp\left(-\frac{1}{N(0)U}\right), \quad (20)$$

where $\Gamma = 3.8 \pm 0.1$, and $N(0) \simeq 0.14$ is the 3d DOS at the Fermi level. Due to the same functional form, the TPSC formalism also predicts an exponential form for T_N with U replaced by U_{sp} . The saturation for $U \gtrsim W$ of U_{sp} to the value $\simeq 3.5$ leads to the saturation of T_N as can be seen in Fig.1. $U_{sp} = U g_{\uparrow\downarrow}$ is not the correct ansatz at large U .

Recently there have been a few controversies concerning the Néel temperature. One of these concerns the relevance of the RPA at weak coupling. [16] [17] A discrepancy was found in an infinite-dimensional approach with $1/d$ corrections in Ref. [16], and in pure 3d formalism in Ref. [17]. From Fig.1 it appears that the TPSC curve merges with RPA results, but only at very small coupling. The modified Stoner criterion used to obtain the Néel temperature in Ref. [17] uses a maximally crossed diagram series which was shown to be not reliable close to half-filling in 2d. [18] Up to $U \simeq W$, TPSC and DMF approaches are very close.

The second controversy [14] concerns the interpretation of the Monte Carlo results: Hasegawa [19] has argued that the Néel temperature extracted from the Monte Carlo simulations was overestimated, in fact it would be rather a mean-field temperature than a true T_N . A indication of this can be seen at large U , where the Monte Carlo is closer to the mean-field result $T_N^{MF} \simeq 6t^2/U$, than to the high temperature series result $T_N^{HT} \simeq 3.83t^2/U$. [20] However, as pointed out by Hirsch [20] this could be also an indication that the itinerant nature of the Hubbard model persists up to large coupling, enhancing the transition temperature. We cannot settle this debate at large U , the TPSC being inappropriate in this regime, but even at low interaction, our results are not very close to the Monte Carlo points.

The U dependence of T_N can be traced back using the self-consistency equation (16). Close to the phase transition the most important contribution is taken into account by the asymptotic form of the susceptibility. At T_N $g_{\uparrow\downarrow} = U_{mfc}/U$, and χ_{sp}^{as} simply reads

$$\chi_{sp}^{as}(q, 0) = \frac{2}{\xi_0^2 U_{sp}} \frac{1}{q^2} \quad , \quad (21)$$

for q measured from \mathbf{Q} . It then follows that the T_N and U dependence of Eq.(16) can be made explicit

$$\frac{1}{2} \frac{U_{mfc}}{U} = R - T_N \frac{1}{\xi_0^2 U_{mfc} \pi^2} \Lambda \quad , \quad (22)$$

where Λ is the radius of the sphere centered on \mathbf{Q} where χ_{sp}^{as} is defined, and R is a short-hand notation for all terms which weakly depend on T_N and U . It has been shown [7] that at low temperature $\xi_0^2 \propto \frac{\partial^2 \chi_0}{\partial q_x^2}$ scales as T^{-2} , in the two-dimensional case. This also holds for the 3d case where

$$\left| \frac{\partial^2 \chi_0}{\partial q_x^2} \right|_{\mathbf{Q}} \simeq \frac{c}{T^2} \quad , \quad (23)$$

with $c = 0.0705$. This behavior extends over a wide temperature domain including T_N . It then follows that

$$\frac{1}{2} \frac{U_{mfc}}{U} = R - \frac{T_N^3}{U_{mfc}^2} \frac{4\Lambda}{c\pi^2} \quad . \quad (24)$$

On the whole range of T_N , the scaling behavior of $U_{mfc} = 2/\chi_0(\mathbf{Q}, 0)$ cannot be neglected and is set, for $T < t$, by $\chi_0(\mathbf{Q}, 0) \simeq 2N(0) \ln(t/T) + \beta$ where $\beta = 0.38$. Equation (24) establishes the Néel temperature saturation.

The TPSC formalism has been shown in $2 < d < 4$ dimensions to be in the same universality class as the Berlin-Kac spherical model, [7] i.e. in the same class as the Heisenberg N -component model with $N \rightarrow \infty$. The corresponding critical exponents in $d = 3$ are: $\nu = 1$, $\gamma = 2$, $\eta = 0$, $\alpha = -1$, $\beta = 1/2$, $\delta = 5$. Furthermore the dynamical exponent has been shown to be $z = 2$. These exponents were also found in the Spin-Hamiltonian approach treated in an Onsager reaction field theory. [21] The size of the critical region, i.e. for which $\xi \gg 1$, is quite narrow. [4] Well above the critical regime, the behavior of ξ^{-1} with T remains roughly linear on the whole temperature range studied up to $T \sim 2t$, even for small U , and does not show any crossover to the RPA regime characterized by $\nu = 1/2$. [22] The linear behavior of ξ^{-1} at high temperature can be ascribed to ξ_0 , (Eqs.(18), (19) and (23)). However for high T , the temperature behavior of $\chi_{sp}^{-1}(\mathbf{Q}, 0)$ is the mean-field one. Indeed, from Eq. (11), we have

$$\chi_{sp}^{-1}(\mathbf{Q}, 0) = \chi_0^{-1}(\mathbf{Q}, 0) - \frac{1}{2} U g_{\uparrow\downarrow} \quad . \quad (25)$$

At high temperature $g_{\uparrow\downarrow}$ slowly increases with T (see next section), and χ_{sp}^{-1} essentially behaves as χ_0^{-1} .

To conclude this section we show in Fig.2 the value of the local moment $\mu^2 = \langle S_i^z S_i^z \rangle$ at T_N as a function of U . TPSC results are compared to DMF results. [11] [12] Due to the saturation of U_{sp} , the moment does not fully develop at large U in contrast with the DMF results and with what is expected from the Heisenberg picture. Nevertheless, up to $U \simeq 8$, TPSC gives a very good agreement compared with $d = \infty$ results.

IV. PARAMAGNETIC PHASE PROPERTIES

The central quantity that determines the magnetic properties of the TPSC approach is the local correlation factor: $g_{\uparrow\downarrow} = \langle n_{\uparrow} n_{\downarrow} \rangle / \langle n_{\uparrow} \rangle \langle n_{\downarrow} \rangle$, which is simply related to the fraction of doubly occupied sites and to the local magnetic moment $\langle S_i^z \rangle = 3(n - \frac{1}{2} n^2 g_{\uparrow\downarrow})$. Furthermore, $g_{\uparrow\downarrow}$ is closely related to the self energy through the following identity [4]

$$\frac{1}{2} \text{Tr} \Sigma G = U \langle n_{\uparrow} n_{\downarrow} \rangle \quad , \quad (26)$$

where G and Σ are respectively the one-particle Green's function and self-energy. From this exact relation, and in spite of the local nature of $g_{\uparrow\downarrow}$, one expects a strong dimensional effect due to the influence of the magnetic fluctuations

on the self-energy Σ in 2d. [4] We are primarily interested in the isotropic 3d case, but we will also comment upon the 2 and anisotropic 3d cases.

In Fig.3 the temperature dependence of $g_{\uparrow\downarrow}$ predicted by TPSC for 3d, is displayed for various values of U . As expected, increasing U is very effective to reduce the fraction of doubly occupied sites. For $U \gtrsim W$, U_{sp} saturates and thus $g_{\uparrow\downarrow} \sim 1/U$ while it should decrease more rapidly with U . In this regime the TPSC approach breaks down. At high temperature $g_{\uparrow\downarrow}$ slowly increases towards 1, whereas on the low temperature side, we are limited to $T > T_N$. The arrows locate T_{min} , the minimum of the curves.

$g_{\uparrow\downarrow}$ has been evaluated in the DMF approach. [23], [2] To make quantitative comparisons between TPSC and DMF results, one needs to use the kinetic energy scale $\sqrt{\langle \epsilon_k^2 \rangle}$. Indeed, within the infinite-dimensional model on the hypercubic lattice, the hopping amplitude is scaled to keep $U/\sqrt{\langle \epsilon_k^2 \rangle}$ finite, whereas the bandwidth is infinite. [24] For a finite dimension d , averaging over the Brillouin zone leads to $\sqrt{\langle \epsilon_k^2 \rangle} = \sqrt{2d}$. In the comparisons of the coupling dependence of $g_{\uparrow\downarrow}$ at two temperatures, a quantitative agreement is found between the TPSC approach and the DMF results as reported in Fig.4. The TPSC curves correspond to $T = 0.6$ and $T = 1.7$, i.e. they surround T_{min} , whereas the infinite-dimensional results extracted from Ref. [23], where $\langle \epsilon_k^2 \rangle = 1/2$, are for $T = 0.175\sqrt{12} \simeq 0.6$, and $T = 0.5\sqrt{12} \simeq 1.73$ respectively. Up to half the bandwidth ($U_{d=\infty} \sim 2$ in $d = \infty$ units), the numerical values are quite close.

In both DMF and 3d-TPSC approaches, a non-monotonous temperature behavior is observed: for U not too strong, $g_{\uparrow\downarrow}$ first begins to decrease before increasing at higher T . The value of the temperature corresponding to this minimum T_{min} marked by an arrow in Fig.3, is plotted in Fig.5 and compared to the infinite-dimensional results. [23], [2] They are quite compatible, since the error bars in Fig.5 for the TPSC results come from the flatness of the curves. For DMF, $T_{min} \rightarrow 0$ for $U \simeq 4\sqrt{12} \simeq 14$, whereas in 3d for $U \gtrsim 10$, $g_{\uparrow\downarrow}$ increases monotonously for $T > T_N$, and cannot be calculated within our approach for $T < T_N$. As discussed by Georges et Krauth, [23] the decrease of $\langle n_{\uparrow}n_{\downarrow} \rangle$ reflects an incipient localization tendency when the temperature increases. This type of behavior is made more acute in the Mott transition, observed for example for the V_2O_3 compound doped with Cr : heating can drive the transition from metal to insulator [25] (but the hypothesis of a structural effect was raised [26]). The same idea is at work in the liquid-solid transition in 3He , in the so-called Pomeranchuk effect: the spin entropy contribution is greater in the solid phase, and increasing the temperature can drive a transition to the solid state.

From Eq.(26) a strong dimensional effect is expected for $g_{\uparrow\downarrow}$, and it becomes interesting to compare the TPSC predictions for 2, 3 and anisotropic 3d cases to the DMF results. To make comparisons between different finite dimensions d , we used again the energy scale $\sqrt{\langle \epsilon_k^2 \rangle}$ rather than naively W , (we first used W and obtained a poor agreement). $\sqrt{\langle \epsilon_k^2 \rangle}$ is a better measure of the kinetic energy: it takes into account not only the bandwidth, but also the particular shape of the density of states. Furthermore, this is the same scaling as the one previously used for comparisons between $d = 3$ and $d = \infty$. In the anisotropic 3d case, the small inter-plane hopping $t_z \ll t$ does not strongly affect the kinetic energy, and as for the 2d case one has $\sqrt{\langle \epsilon_k^2 \rangle} = 2$.

In Fig.6, we show the temperature dependence of $g_{\uparrow\downarrow}$ for the two, isotropic and anisotropic three-dimensional cases in the TPSC approach. The units on the figure are the 3d ones. We first focus on the 2 and isotropic 3d cases. The values of $g_{\uparrow\downarrow}$ cannot be distinguished for 2 and 3d at high temperature. At a temperature close to the arrows locating the minimum of the isotropic 3d case, the curves separate. At low temperature in 2d, U_{sp} goes down when T decreases. This behavior is confirmed by Monte Carlo calculations for the double occupation factor, [27] [28] and is a manifestation of the incipient antiferromagnetic fluctuations, as can be seen by inspection of Eq.(13): the increase of the spin susceptibility integral, leads to a decrease of the double occupation factor. This behavior is not clearly seen in the 3d case due to the very narrow range of the critical regime, and to the smaller effect of fluctuations in high dimensions. The temperature at which the 2 and 3d behaviors separate, close to T_{min} , is higher than the crossover temperature which marks the entering of the critical regime characterized by a large correlation length, [29] i.e. ξ does not need to be large to see a strong dimensional effect. The non-monotonous temperature behavior of $g_{\uparrow\downarrow}$ observed in 3d and $d = \infty$ cases, is also present but much less important in the 2d case for small interaction values, as revealed by a careful inspection of Fig.6 for $U = 2$. In 2d the strong antiferromagnetic fluctuations prevent a sensible increase of $g_{\uparrow\downarrow}$ when the temperature decreases.

In the anisotropic 3d case, a small inter-plane hopping t_z can stabilize the ordered phase, but has no effect on the value of $g_{\uparrow\downarrow}$, as shown in Fig.6 for $U = 4$, and $t_z = 10^{-3}$ (3d units): for $T > T_N(t_z) \sim 0.18$ the 2d and anisotropic 3d curves cannot be distinguished. This behavior is a manifestation of the fact that for these U and t_z values, the Néel transition takes place in the incoherent 3d one-particle motion regime: the first fermionic Matsubara frequency πT_N is much higher than t_z . The inter-plane hopping having no effect on the one-particle Green's function and self-energy, it follows from Eq. (26), that the behavior of $g_{\uparrow\downarrow}$ is dominated by two-dimensional effects, even if the critical exponents are the same for the isotropic and anisotropic 3d models.

In the high temperature regime (typically for $T > T_{min}$), when the dimension does not have any influence, one can expect that a simple two-site problem may be instructive. The calculation of $g_{\uparrow\downarrow}$ in the two-site case is detailed

in the appendix, we list here the main results. The two-site problem solved in the Grand-canonical ensemble, with a chemical potential fixed to the half-filling value, gives a good quantitative agreement for the double occupation factor in comparisons with the TPSC, at high temperature, for low and moderate interaction values. The two site results also display a non monotonous temperature behavior for $g_{\uparrow\downarrow}$ with a U -dependent minimum. This minimum is pushed to high temperature when U increases, in contrast with what was observed in the TPSC and DMF approaches (Fig.5). However if we freeze the charge fluctuations which are important in a 2 site problem, working in the canonical ensemble, the decrease of T_{min} when U increases is recovered.

From the comparisons between 2d, 3d, $d = \infty$, and the two site case, it appears that the non-monotonous temperature behavior of $\langle n_{\uparrow}n_{\downarrow} \rangle$ is not a purely dimensional effect, nor a strong U effect, and that it is overcome by strong antiferromagnetic fluctuations in $d = 2$.

Finally, we compare our results on finite-size lattices with Monte Carlo calculations. In Fig.7, we compare our results for $\mu^2 = \langle S_i^z S_i^z \rangle$ to the Monte Carlo results of Hirsch [20] on a 4^3 lattice at $T = 0.5$. The TPSC calculations are also done on a 4^3 lattice. Clearly up to half the bandwidth, the results are quite compatible. In Fig.8 we have plotted the staggered susceptibility as a function of the site number (4,6,8 and 10^3), for different temperatures and for $U = 6$. These are compared with the Monte Carlo results of Scalettar *et al.* [10] An overall agreement can be observed except at $T = 0.4$ for the intermediate sizes. In the TPSC and in Monte Carlo calculations, a size effect is clearly seen at this temperature, however for Monte Carlo, the linear dependence of $\chi_{sp}(\mathbf{Q}, 0)$ is the signature of an "ordered" phase, whereas the transition is not reached yet in TPSC.

V. CONCLUSION

The TPSC approach has been shown in the isotropic 3d case, to give compatible results in comparison with $d = \infty$ calculations, for the Néel temperature as well as for the local correlation function $\langle n_{\uparrow}n_{\downarrow} \rangle$. The comparisons with Monte Carlo calculations from low up to intermediate coupling regime, except for the Néel temperature which is systematically larger in Monte Carlo, are remarkable.

The various results for $\langle n_{\uparrow}n_{\downarrow} \rangle$ obtained primarily for 3d, but also compared to 2 and anisotropic 3d Hubbard models shed light on the applicability of the DMF approach. The latter compares very well with the isotropic 3d case for $\langle n_{\uparrow}n_{\downarrow} \rangle$, which is a local quantity that depends on the dimensionality. That may be seen through Eq.(26). However, due to the strong \mathbf{k} -dependence of Σ , the 2d case, or the anisotropic 3d case for which the Néel transition can be reached with a purely two-dimensional self-energy, are out of reach of the $d = \infty$ model, as long as the $1/d$ corrections are not taken into account in a satisfactory manner. Progress in that direction has been achieved recently. [30]

Finally, let us stress the fact that up to intermediate coupling, the TPSC gives the same agreement in 2 and 3d, and thus is able to capture the essence of two very different physical systems. This method is not restricted to half-filling, nor to the hypercubic case, in contrast with many other approaches. It then follows that the frustrated antiferromagnetism as well as the metallic ferromagnetism can be considered. Furthermore a generalization of this approach can be elaborated in an ordered phase. Work in that direction is in progress.

It's a pleasure to thank A.-M. S. Tremblay, J.-L. Richard and S. Pairault for enlightening discussions and key ideas. We are indebted to Yuri Vilk for providing us with his code enabling the calculations in 2d, and to Steve Allen for sharing his Monte Carlo calculation results.

APPENDIX A: TWO-SITE RESULTS

In this appendix we detail the calculations of the double occupation factor for the 2 site problem. From the comparisons between the 2d, isotropic and anisotropic 3d, and $d = \infty$ results, presented in the main text, and the observation that, when properly scaled, $\langle n_{\uparrow}n_{\downarrow} \rangle$ does not depend on the dimension at high T , we expect a good quantitative agreement between the 2 site problem and the infinite lattice results for any dimensions at high temperature. Apart from a quantitative agreement, it will be shown that this simple problem roughly explains the non-monotonous behavior of $g_{\uparrow\downarrow}$ as a function of T , and the U -dependence of T_{min} observed in the 3d and $d = \infty$ lattice case.

Considering a two-site problem, with a chemical potential $\mu = U_{2 \text{ sites}}/2$, fixed to have a mean occupation number per site $n = 1$, it is a straightforward exercise to diagonalize the Hamiltonian, and to evaluate the double occupation factor. The results for $g_{\uparrow\downarrow}$ for this problem are presented in Fig.9 as a function of temperature and various values of the interaction, along with the 3d TPSC results. As previously done for comparisons between different dimensions, interaction and temperature can be rescaled for quantitative comparisons. With the periodic boundary conditions for the two sites problem, the kinetic measure is $\sqrt{\langle \epsilon_k^2 \rangle} = 2$, as in 2d. For low and moderate repulsion, and for a temperature typically higher than the 3d T_{min} , both results are close. The 2 site case not only provides a rough

quantitative agreement, but also displays a non-monotonous behavior as a function of temperature. This one can be easily understood in terms of eigenvalues ϵ and eigenstates. In Fig.10 we have plotted the different values of $\epsilon - \mu N$ as a function of $U_{2 \text{ sites}}$. Table 1 gives a schematic description of the corresponding states and their contribution to $\langle n_{\uparrow} n_{\downarrow} \rangle$.

Index	degeneracy	$\epsilon - \mu N$	$\langle \phi n_{\uparrow} n_{\downarrow} \phi \rangle$
a	1	$\frac{U}{2} - \frac{1}{2}\sqrt{U^2 + 64t^2} - 2\mu$	$\frac{1}{4} - \frac{1}{4}\frac{U}{\sqrt{U^2 + 64t^2}}$
b	3	-2μ	0
c	2	$-2t + U - 3\mu$	1/2
	2	$-2t - \mu$	0
d	2	$2t + U - 3\mu$	1/2
	2	$2t - \mu$	0
e	1	$U - 2\mu$	1/2
	1	$2U - 4\mu$	1
	1	0	0
f	1	$\frac{U}{2} + \frac{1}{2}\sqrt{U^2 + 64t^2} - 2\mu$	$\frac{1}{4} + \frac{1}{4}\frac{U}{\sqrt{U^2 + 64t^2}}$

TABLE 1. Details of Fig.10. Index refers to the different letters indexing the curves in Fig.10. For each curve we specify the degeneracy order, and the value of $\epsilon - \mu N$, the number of electrons being the coefficient of μ . The last column gives the value of the double occupation operator in each state. For example the curve c corresponds to 2 three-electron states, with $\langle \phi | n_{\uparrow} n_{\downarrow} | \phi \rangle = 1/2$ for each, and to 2 one-electron states with no double occupation.

For $U_{2 \text{ sites}} < 4$, the first excited state is four-fold degenerate and corresponds to charge fluctuations (the particle number is not the same as in the ground state). Two of these four states correspond to a non-zero double occupation. For higher interaction the first excited state is three-fold degenerate, corresponding to spin fluctuations, and has no double occupation. Thus for $U_{2 \text{ sites}} > 4$ the simple 2 site problem predicts a non-monotonous temperature dependence of $\langle n_{\uparrow} n_{\downarrow} \rangle$. In that case the distance between the first and second excited states raises with interaction as can be seen in Fig.10. It follows that the temperature at which the double occupation factor begins to increase, grows with the repulsion. This contrasts with the behavior observed in $d = 3$ or $d = \infty$. Nevertheless, the simple 2 sites problem favors charge fluctuations compared with the thermodynamic limit, and interestingly the decrease of T_{min} with an increase of U , is recovered if we freeze charge fluctuations taking 2 sites with precisely 2 electrons. If freezing charge fluctuations gives a qualitative agreement for T_{min} as a function of U , the quantitative agreement for $g_{\uparrow\downarrow}$ in comparisons with the infinite lattice case is not as good as it was with charge fluctuations allowed.

¹ For correspondence, email: dare@lrc.univ-mrs.fr

- [1] A. Georges, G. Kotliar, Phys. Rev. B **45**, 6479 (1992).
- [2] A. Georges, G. Kotliar, W. Krauth, and M. Rozenberg, Rev. Mod. Phys. **68**, 13 (1996).
- [3] Y.M. Vilks, Liang Chen, A.-M.S. Tremblay, Phys. Rev. B **49**, 13 267 (1994).
- [4] Y. M. Vilks and, A.-M. S. Tremblay, J. Phys. I France **7**, 1309 (1997).
- [5] A. Veilleux, A.-M. Daré, Liang Chen, Y.M. Vilks, and A.-M.S. Tremblay, Phys. Rev. B **52**, 16255 (1995).
- [6] G. Baym and L.P. Kadanoff, Phys. Rev. **124**, 287 (1961). G. Baym, Phys. Rev. **127**, 1391 (1962).
- [7] A.-M. Daré, Y. M. Vilks, and A.-M. S. Tremblay, Phys. Rev. B **53**, 14236 (1996).
- [8] Leo P. Kadanoff and Gordon Baym *Quantum statistical Mechanics*, Addison Wesley, 1989, Chap. 5.
- [9] N.E. Bickers and D.J. Scalapino, Annals of Physics, **193**, 206 (1989).
- [10] R.T. Scalettar, D.J. Scalapino, R.L. Sugar, and D. Toussaint, Phys. Rev. B **39**, 4711 (1989).
- [11] M. Jarrell, Phys. Rev. Lett **69**, 168 (1992).
- [12] M. Jarrell, and Thomas Prushke, Z. Phys. B **90** 187 (1993).
- [13] Avinash Singh, electronic archives cond-mat/9802047.
- [14] Yolande H. Szczech, Michael A. Tusch, and David E. Logan, Phys. Rev. Lett **74**, 2804 (1995).
- [15] Michael A. Tusch, Yolande H. Szczech, and David E. Logan, Phys. Rev. B **53**, 5505 (1996).
- [16] P. G. J. van Dongen, Phys. Rev. Lett **67**, 757 (1991), Phys. Rev. B **50**, 14016 (1994).
- [17] A.N. Tahvildar-Zadeh, J.K. Freericks, M. Jarrell, Phys. Rev. B **55**, 942 (1997).
- [18] Liang Chen, C. Bourbonnais, T. Li, and A.-M. S. Tremblay, Phys. Rev. Lett **66**, 369 (1991).
- [19] H. Hasegawa J. Phys. Condens. Matter **1**, 9325 (1989).

- [20] J.E. Hirsch, Phys. Rev. B **35**, 1851 (1987).
 [21] D. E. Logan, Y. H. Szczech, and M. A. Tusch, Europhys. Lett. **30**, 307 (1995).
 [22] We thank C. Bourbonnais for discussion on this point.
 [23] Antoine Georges, and Werner Krauth, Phys. Rev. B **48**, 7167 (1993).
 [24] W. Metzner and D. Vollhardt, Phys. Rev. Lett **62**, 324 (1989).
 [25] D.B. McWhan, J.P. Remeika, T.M. Rice, W.F. Brinkman, J.P.Maita, and B.A. Menth, Phys. Rev. Lett **27**, 941 (1971);
 D.B. McWhan, B.A. Menth, J.P. Remeika, W.F. Brinkman, and T.M. Rice, Phys. Rev. B **7**, 1920 (1973).
 [26] Ross H. McKenzie, Comments Cond. Mat. Phys, **18**, 309 (1998).
 [27] S. Allen, private communication.
 [28] S. Pairault, D. Sénéchal, and A.-M. S. Tremblay, electronic archives cond-mat/9905242.
 [29] For the 2d crossover temperature, see Fig.3 from Ref. [4].
 [30] M.H. Hettler, A.N. Tahvildar-Zadeh, M. Jarrell, T. Pruschke, and H.R. Krishnamurthy, Phys. Rev. B **58**, R7475 (1998).
 M. S. Laad, and M. van den Bossche, electronic archives cond-mat/9802176.

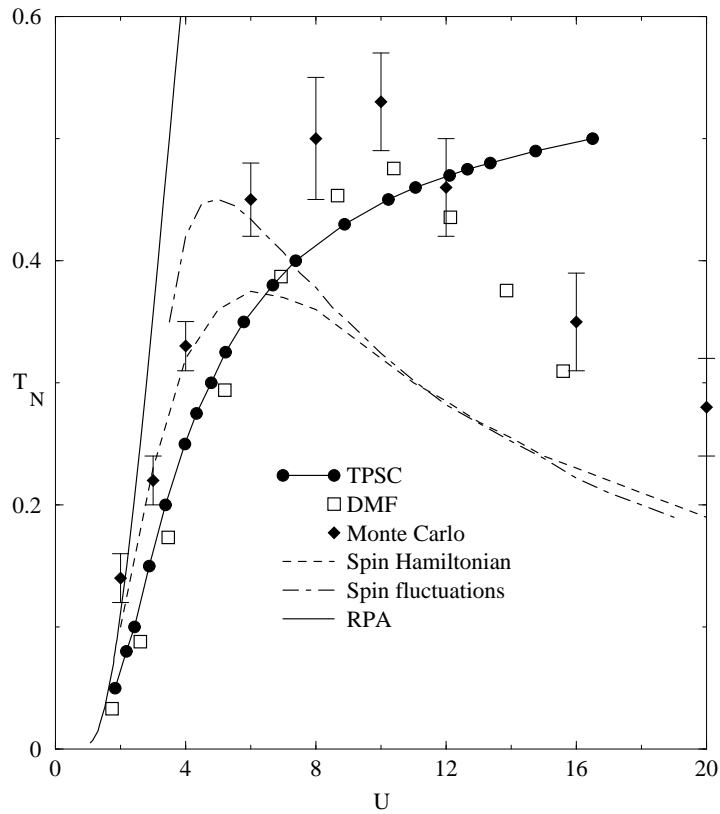


FIG. 1. Néel temperature as a function of U , for the TPSC formalism compared with other approaches, see text.

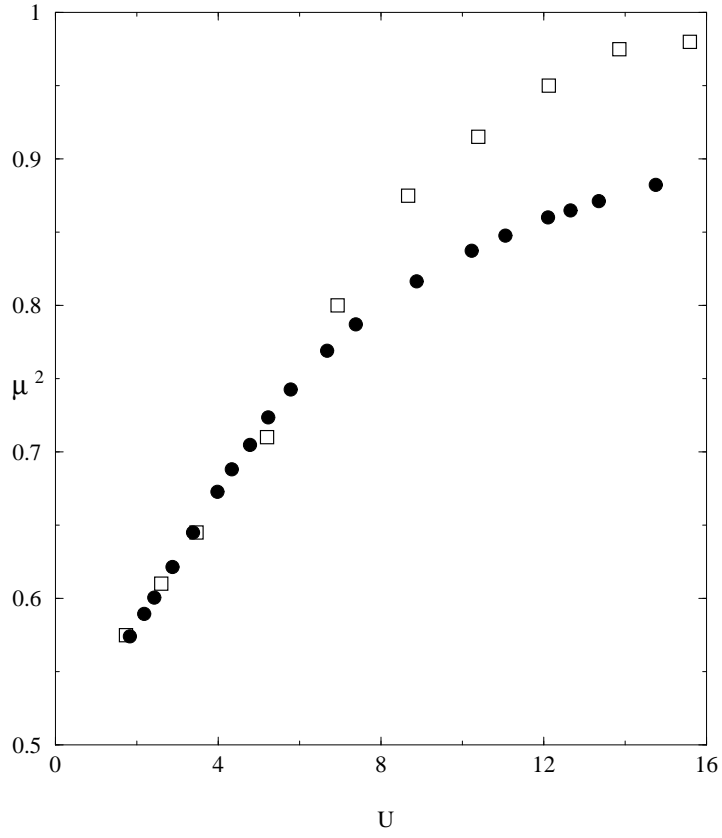


FIG. 2. $\mu^2 = \langle S_i^z S_i^z \rangle$ at T_N as a function of U . Black circles correspond to the $d = 3$ case, while open symbols are DMF results, extracted from Ref. [11]. The energy unit is the 3d one.

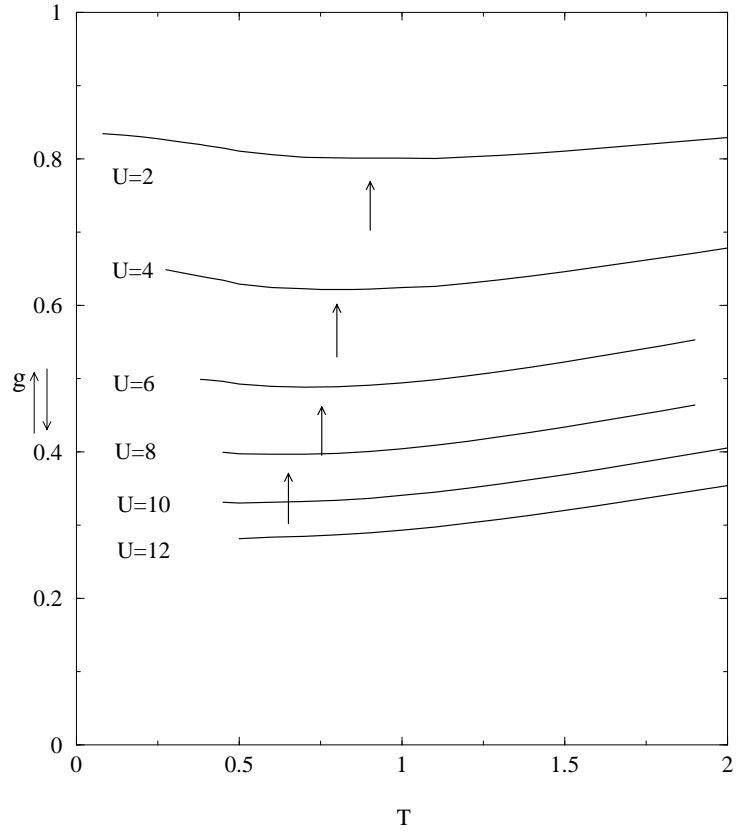


FIG. 3. Double occupation factor $g_{\uparrow\downarrow} = \langle n_{\uparrow}n_{\downarrow} \rangle / \langle n_{\uparrow} \rangle \langle n_{\downarrow} \rangle$ as a function of temperature for different values of the on-site repulsion. The arrows locate the minimum of the curves.

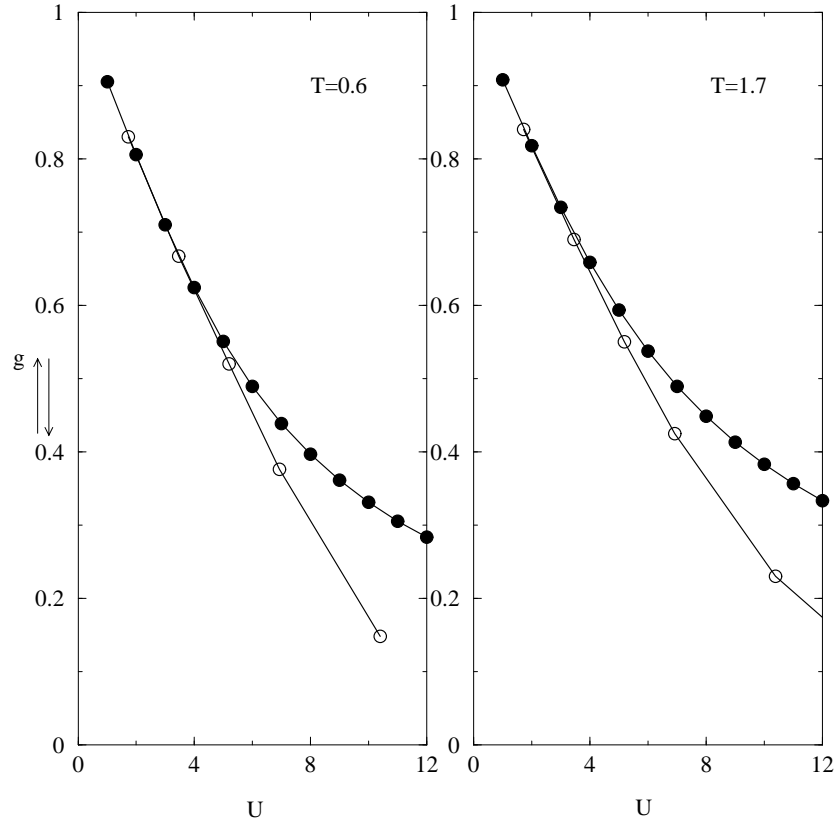


FIG. 4. Comparisons between 3d-TPSC and DMF for $g_{\uparrow\downarrow}$ as a function of U for two different temperatures. Black circles correspond to the $d = 3$ case, while open symbols are DMF results, extracted from Ref.[23]. The energy unit is the 3d one.

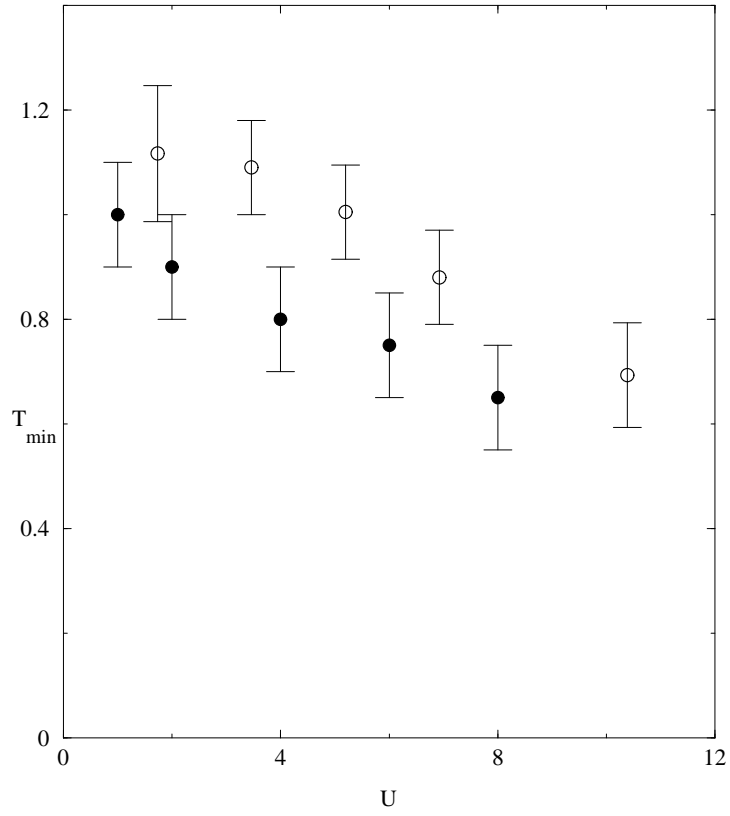


FIG. 5. Temperature corresponding to the minimum of $g_{\uparrow\downarrow}(T)$ for the 3d Hubbard model compared to the DMF results extracted from Ref.[23]. Black circles are for 3d-TPSC, open symbols for DMF results. The energy unit is the 3d one.

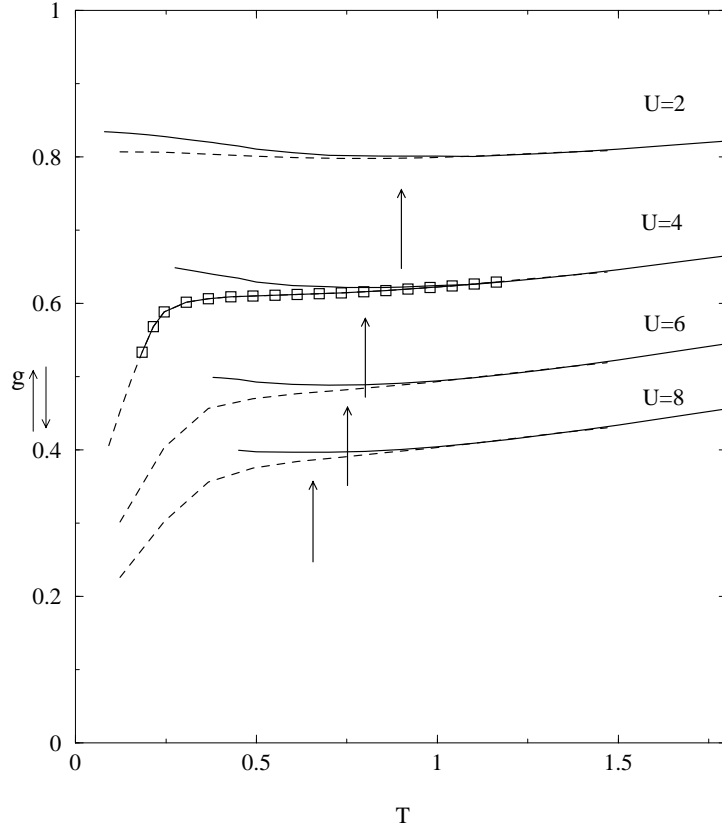


FIG. 6. Comparisons between $d = 3$, $d = 2$, and the anisotropic 3d cases for $g_{\uparrow\downarrow}$ as a function of T , and different U values. The energy unit is the 3d one (see text). Solid line corresponds to 3d, the dashed one to 2d. Square symbols are for the anisotropic 3d case, with $t_z = 10^{-3}$ and $U = 4$, this curve ends up at $T_N(t_z) \sim 0.18$. The arrows locate the minimum of the 3d curves.

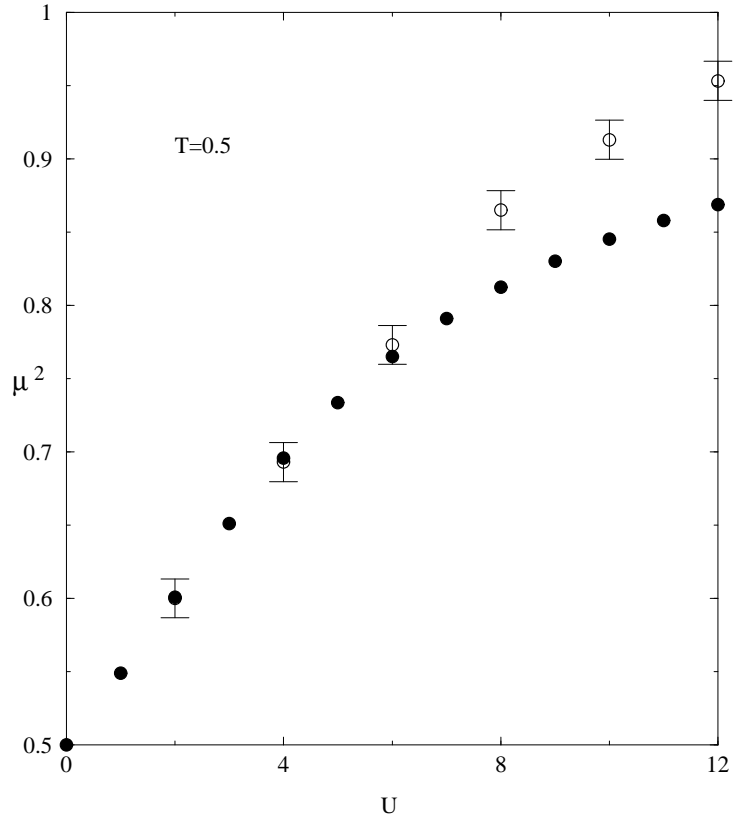


FIG. 7. $\mu^2 = \langle S_i^z S_i^z \rangle$ at $T = 0.5$ as a function of U . Black circles correspond to the TPSC results on a 4^3 lattice, open symbols are the Monte Carlo results on a 4^3 lattice, extracted from Ref.[20]

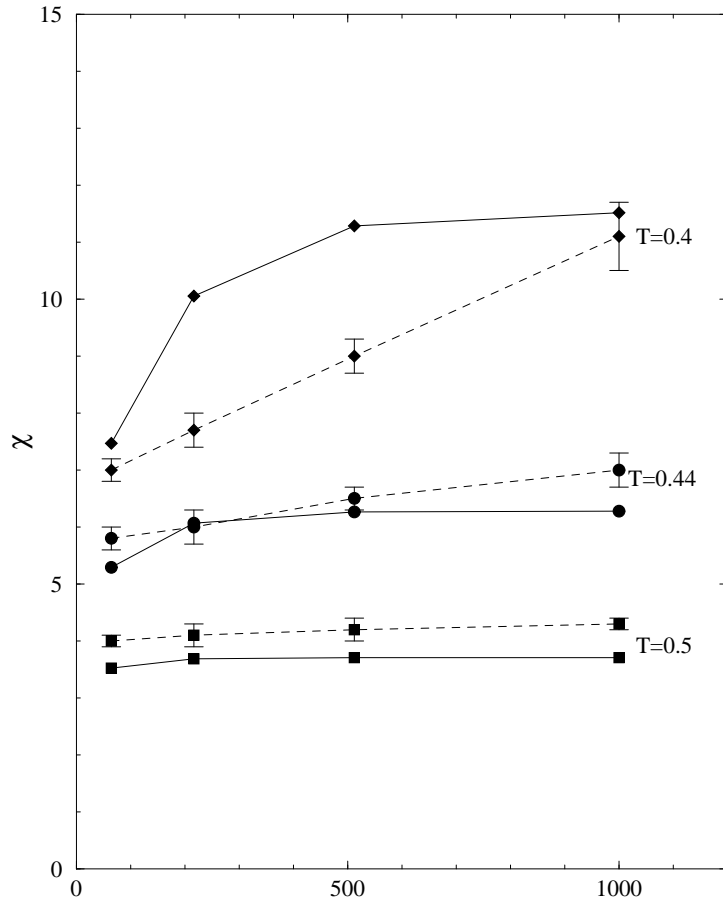


FIG. 8. $\chi_{sp}(\mathbf{Q}, 0)$ at $U = 6$ and different T values, as a function of the number of lattice sites. Symbols with error bars, linked by dashed lines are Monte Carlo results from Ref.[10], while symbols linked by solid lines are the TPSC results.

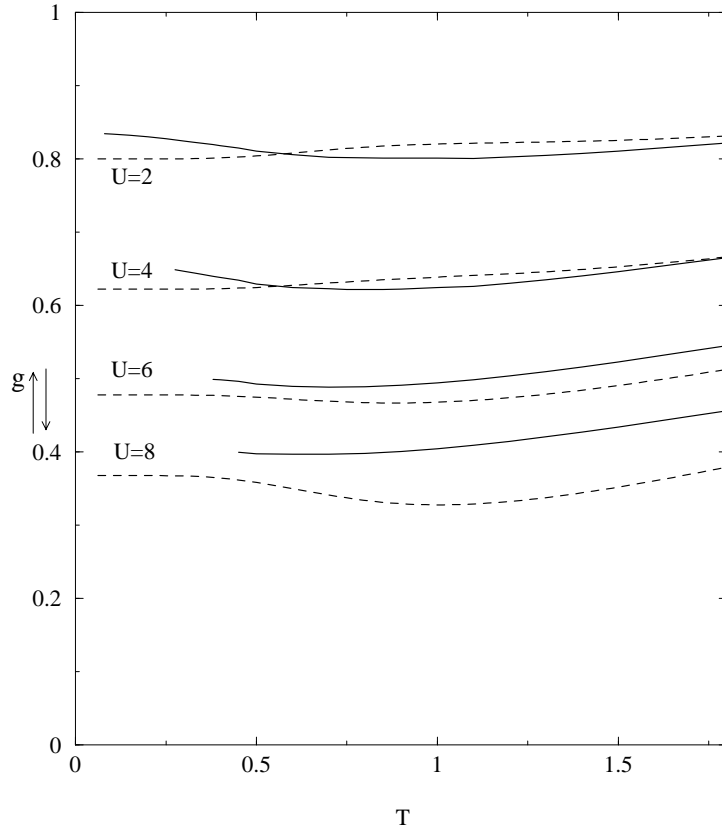


FIG. 9. $g_{\uparrow\downarrow}$ as a function of temperature for different values of the on-site repulsion (solid line) compared to the two-site result (dashed line).

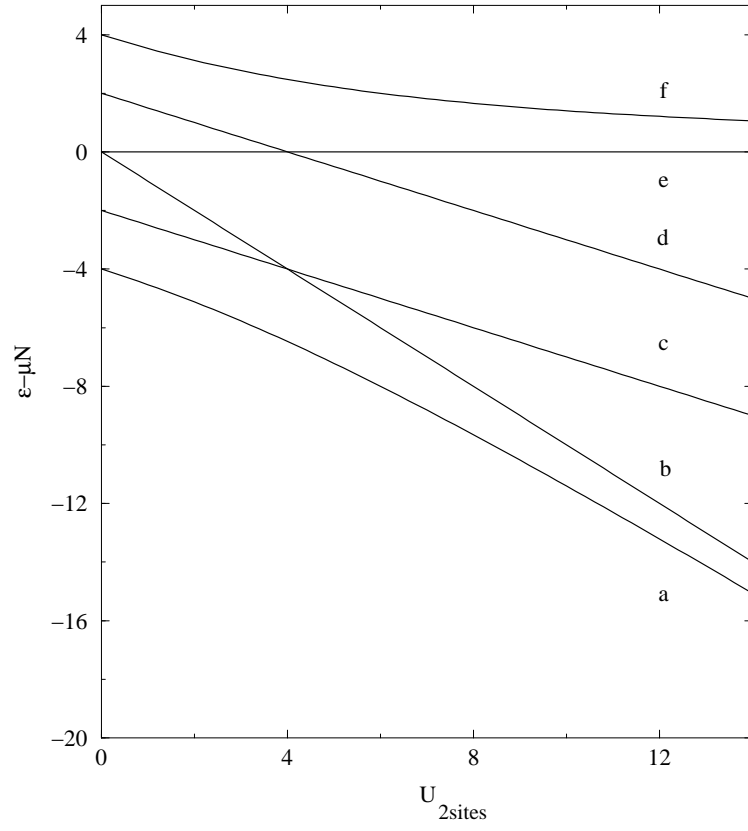


FIG. 10. Eigenvalues of the two-site problem $\epsilon - \mu N$ as a function of the on-site repulsion. Details about these states can be found in Table 1.